J. Fluid Mech. (2000), *vol.* 425, *pp.* 111–132. Printed in the United Kingdom

Theoretical and experimental investigation of the compression wave generated by a train entering a tunnel with a flared portal

By M. S. HOWE[1], M. IIDA[2], T. FUKUDA[2] AND T. MAEDA[2]

[1]Boston University, College of Engineering, 110 Cummington Street, Boston MA 02215, USA

[2]Railway Technical Research Institute, 2-8-38 Hikari-cho, Kokubunji-shi, Tokyo 185-8540

(Received 14 February 2000 and in revised form 10 July 2000)

The compression wave generated by a high-speed train entering a tunnel is studied theoretically and experimentally. It is shown that the pressure rise across the wavefront is given approximately by

$$\frac{\rho_o U^2}{1-M^2}\frac{\mathscr{A}_o}{\mathscr{A}}\left(1+\frac{\mathscr{A}_o}{\mathscr{A}}\right),$$

where ρ_o, U, M, $\mathscr{A}_o$ and $\mathscr{A}$ respectively denote the mean air density, train speed, train Mach number, and the cross-sectional areas of the train and the uniform section of the tunnel. A monopole source representing the displacement of air by the train is responsible for the main pressure rise across the wave, but second-order dipole sources must also be invoked to render theoretical predictions compatible with experiment. The principal dipole is produced by the compression wave drag acting on the nose of the train. A second dipole of comparable strength, but probably less significant in practice, is attributed to 'vortex sound' sources in the shear layers of the back-flow out of the tunnel of the air displaced by the train.

Experiments are performed that confirm the efficacy of an 'optimally flared' portal whose cross-sectional area $S(x)$ varies according to the formula

$$\frac{S(x)}{\mathscr{A}} = 1\Big/\left[\frac{\mathscr{A}}{\mathscr{A}_E}-\frac{x}{\ell}\left(1-\frac{\mathscr{A}}{\mathscr{A}_E}\right)\right], \quad -\ell < x < 0,$$

where x is distance increasing negatively into the tunnel, ℓ is the prescribed length of the flared section, and $\mathscr{A}_E$ is the tunnel entrance cross-sectional area, given by

$$\frac{\mathscr{A}_E}{\mathscr{A}} = \left(\frac{\ell}{2R}\right)^{2/3}\left[\left(1+\sqrt{1-\left(\frac{2R}{3\sqrt{3}\ell}\right)^2}\right)^{1/3}+\left(1-\sqrt{1-\left(\frac{2R}{3\sqrt{3}\ell}\right)^2}\right)^{1/3}\right]^2, \quad R=\sqrt{\frac{\mathscr{A}}{\pi}}.$$

This portal is predicted theoretically to cause the pressure to increase linearly with distance across a compression wavefront of thickness $\sim \ell/M$, which is very much larger than in the absence of flaring. The increased wave thickness and linear pressure variation counteract the effect of nonlinear steepening of the wave in a long tunnel, and tend to suppress the environmentally harmful 'micro-pressure wave' radiated from the far end of the tunnel when the compression wave arrives. Our experiments are conducted at model scale using axisymmetric 'trains' projected at $U \sim 300$ k.p.h. ($M \approx 0.25$) along the axis of a cylindrical tunnel fitted with a flared portal. The blockage $\mathscr{A}_o/\mathscr{A} = 0.2$, which is comparable to the larger values encountered in high-speed rail operations.

1. Introduction

A high-speed train entering a tunnel compresses the stationary air immediately in front of it, causing most of the displaced air to flow over the train and out of the tunnel portal. The pressure rise propagates into the tunnel (ahead of the train) at the speed of sound as a compression wave whose amplitude is typically 1–3% of atmospheric pressure when the train Mach number M exceeds about 0.2 ($\sim$ 250 k.p.h.) (figure 1). The initial shape of the wavefront profile depends critically on the geometry of the tunnel entrance portal and on the 'blockage', i.e. the ratio $\mathscr{A}_0/\mathscr{A}$ of the train cross-sectional area $\mathscr{A}_0$ to the cross-sectional area $\mathscr{A}$ of the uniform section of the tunnel (Hara 1961; Hara *et al.* 1968; Ozawa, Tsukamoto & Maeda 1976; Ozawa & Maeda 1988; Ozawa *et al.* 1991; Ozawa 1979; Woods & Pope 1976; Ogawa & Fujii 1994, 1997; Howe 1998*a*, *b*, 1999*a*). The pressure rise across the wavefront $\sim \rho_0 U^2 \mathscr{A}_0/\mathscr{A}$, where ρ_0 is the mean air density and U denotes train speed; for a uniform tunnel of constant diameter D the wavefront thickness is of order $D/M \leqslant 5D$.

A rarefaction wave is generated as the tail of the train enters the tunnel. In a long tunnel multiple reflections of the waves from either end, and from tunnel 'discontinuities' such as changes in cross-sectional area, air shafts, side branches, etc., and also from the nose and tail of the train, produce complicated interference patterns with the possibility of locally intense pressure transients. The rapidly varying changes in pressure can cause discomfort to passengers in unsealed rail cars and to maintenance personnel in the tunnel. The reflection of the compression wave from the distant tunnel exit is accompanied by the emission from the tunnel of a pressure pulse (the *micro-pressure wave* of figure 1). The strength of this pulse is proportional to the steepness of the compression wavefront at the exit; for tunnels longer than about 3 km with modern concrete slab tracks (offering little dissipation to the propagating wave) nonlinear steepening of the compression wavefront as it propagates along the tunnel can cause the micro-pressure wave amplitude to be as large as 50 Pa near the exit. This is comparable to the sonic boom overpressure from a supersonic aircraft, and frequently rattles windows of neighbouring buildings and is responsible for much environmental annoyance. Nonlinear steepening in a long tunnel tends to be inhibited by relaxation processes if the initial thickness of the compression wave is sufficiently large (Ozawa *et al.* 1991; Maeda *et al.* 1993; Iida *et al.* 1996). Considerable efforts have therefore been made (many of which are summarized by Ozawa *et al* 1991) to enhance the initial wave thickness by judicious design of the train nose profile and tunnel portal. This problem must be resolved if the full benefits of sustained high-speed travel are to be realized; the solution is made more desirable by the introduction of 500 k.p.h. *Maglev* trains on new routes that typically require up to 50% of a journey to be within a tunnel.

Large increases in the initial wave thickness are currently obtained by the installation of a tunnel entrance 'hood', that can extend as far as 50 m ahead of the tunnel entrance. For example, a fivefold increase in wave thickness is achieved by the 49 m long hood at the eastern entrance to the Ohirayama tunnel in Japan (Ozawa *et al.* 1991). The compression wave begins to form as the train enters the hood: the wave thickness is increased by venting high-pressure air through 'windows' in the walls of the hood. The optimum distribution of these windows is determined from scale model tests (of the type described later in this paper), usually involving a 'tunnel' consisting of a thin-walled, circular cylindrical tube, and axisymmetric 'trains' projected along a very tight guide-wire extending along the tube axis.

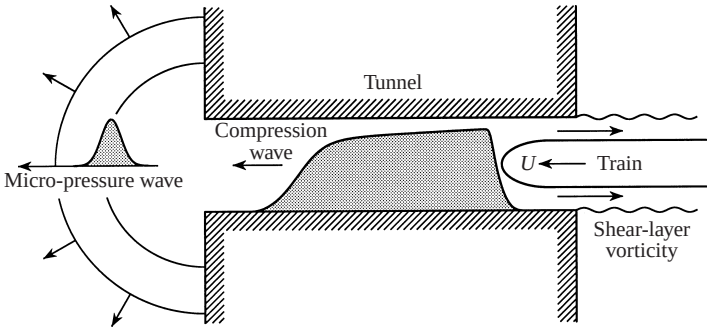

FIGURE 1. Schematic illustration of a train entering a tunnel, showing the compression wave, the micro-pressure wave, and the shear layers of the exit flow from the tunnel entrance portal.

However, entrance hoods tend to be unsightly and alternative tunnel portal modifications have therefore been considered. It has been demonstrated numerically by Fox & Vardy (1973) and experimentally by Ozawa *et al.* (1976) and Ozawa (1979) that flaring of the tunnel portal could lead to large increases in the initial compression wave thickness. The most desirable form for the compression wave profile is one in which the pressure increases linearly with distance across the wavefront, with a constant pressure gradient that is as small as practicable. This would not only delay the onset of a nonlinearly steepened wavefront, but also would inhibit the formation of high-frequency 'shocklets' on an otherwise extended, but roughened wavefront. The cross-sectional area of an optimally flared tunnel portal must vary in an appropriate manner with distance from the tunnel inlet plane; the constant pressure gradient would then equal $M\Delta p/\ell$, where Δp is the overall pressure rise (which is independent of portal geometry) and ℓ is the length of the flared section of the tunnel. An analytical expression for this optimal flaring was derived by Howe (1999*b*) from a linear theory of compression wave formation, which was based on the assumption that the blockage $\mathscr{A}_o/\mathscr{A}$ is small.

Linear theory predictions for a *non-flared* portal are found to be in good agreement with model scale experiments provided $\mathscr{A}_o/\mathscr{A}$ does not exceed about 0.12 (Howe 1999*a*). However, high-speed rail operations in practice involve $\mathscr{A}_o/\mathscr{A}$ as large 0.2 or slightly higher, and it is therefore important to seek an extension of the linear theory to cover such cases, and to validate predictions by comparison with experiment. These objectives are the subject of this paper.

The equation of vortex sound generation in an homentropic fluid (Howe 1998*a*) is applied to determine a second-order approximation (in powers of $\mathscr{A}_o/\mathscr{A}$) to the theory of compression wave formation. Linear theory replaces the train by a system of monopole sources distributed over the nose and tail sections, where the cross-sectional area varies; these sources account for most of the pressure rise across the wavefront. The most important second-order sources consist of *dipoles* orientated parallel to the train and distributed over the nose and tail, with strength determined by the surface pressure; a somewhat smaller contribution is also made by 'vortex dipoles' in the free shear layer of the air ejected from the tunnel portal by the entering train. Additional vortex sources occur in the boundary layer on the moving train, and also possibly in regions of flow separation; but these are not easily quantified because they depend critically on train nose geometry. A principal conclusion of our analysis is that the linear-theory, optimally flared portal remains optimal to second order in the blockage $\mathscr{A}_o/\mathscr{A}$. This prediction is confirmed by the model scale tests described in this paper at train Mach numbers ~ 0.25 (~ 300 k.p.h.) and $\mathscr{A}_o/\mathscr{A} = 0.2$.

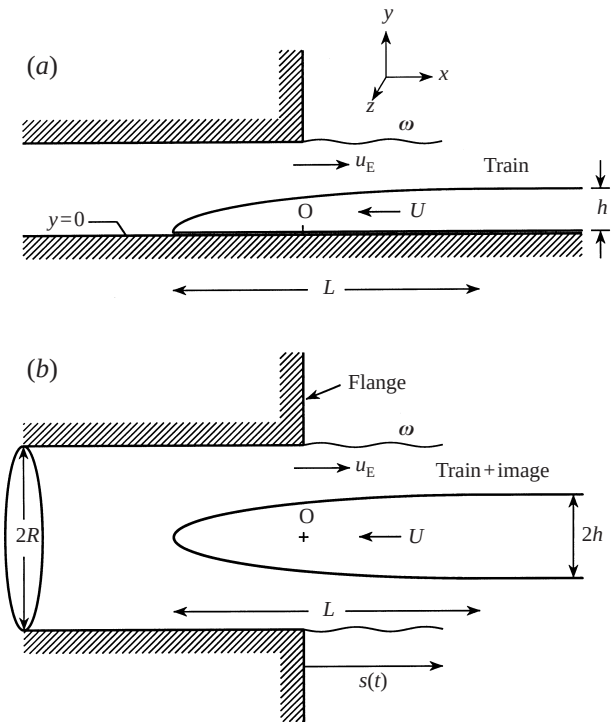

FIGURE 2. (*a*) Train entering tunnel. (*b*) Dynamically equivalent configuration consisting of the train and its image in the ground plane entering a flanged duct formed by the reflection of the tunnel walls in the ground plane.

The second-order theory of compression wave formation and its application to the flared portal are discussed in §§ 2 and 3. A detailed description of the model scale experiments and measurement procedure is given in § 4. However, to avoid interruption of the natural flow of the discussion, it is convenient to make forward references in §§ 2, 3 to the results of these measurements, and to include in these sections a general discussion of the comparison of theory and experiment. Steady-state predictions of the second-order theory (which become relevant after the nose of the train has passed into the tunnel) are compared in § 2 with Hara's gas dynamic theory of the overall pressure rise across the wavefront (Hara 1961; Hara *et al.* 1968). This comparison isolates that part of the Hara prediction formula that corresponds to the pressure rise produced by the free-shear vortex dipoles, which are often not relevant in practice because their influence is not usually felt until such times that additional, extraneous pressure rises attributable to boundary layer growth (and perhaps separation) on the train and interior tunnel wall (both neglected in Hara's gas dynamic formula) are also important.

2. Theory of compression wave generation

2.1. *The governing equations*

The dynamics of the formation of the compression wave of figure 1 by an entering train are equivalent to those of the simpler problem depicted in figure 2(*a*), in which the tunnel is replaced by a semi-infinite duct. To fix ideas we shall consider first a

tunnel of uniform cross-sectional area $\mathscr{A}$. Let the train be travelling at constant speed U in the negative x-direction of the rectangular coordinates $\boldsymbol{x} = (x, y, z)$, where the origin is at O at ground level in the entrance plane of the tunnel, with the x-axis lying in the vertical plane of symmetry. The pressure, density and speed of sound in the air are denoted respectively by $\bar{p}$, ρ and c. They vary with position $\boldsymbol{x}$ and time t within the tunnel, and their corresponding undisturbed values are p_o, ρ_o, c_o.

The cross-section of the train is assumed to become uniform with constant area $\mathscr{A}_\mathrm{o}$ at a distance L from the nose. The uniform maximum height of the train is h, and the aspect ratio of the nose h/L is taken to be sufficiently small, and the train profile sufficiently streamlined, to ensure that flow separation does not occur. In practice the Mach number $M = U/c_\mathrm{o}$ does not exceed about 0.4, and the blockage $\mathscr{A}_o/\mathscr{A}$ is typically less than about 0.2. Heat transfer and frictional losses will be neglected during the initial stages of wave formation. The air flow may then be regarded as homentropic (so that $\rho \equiv \rho(\bar{p})$) and the compression wave can be calculated from the corresponding equation describing the generation of sound in the presence of a moving surface, which we take in the form (Howe 1975, 1998*a*)

$$\left(\frac{\mathrm{D}}{\mathrm{D}t}\left(\frac{1}{c^2}\frac{\mathrm{D}}{\mathrm{D}t}\right) - \frac{1}{\rho}\nabla\cdot(\rho\nabla)\right) B = \frac{1}{\rho}\nabla\cdot(\rho\boldsymbol{\omega}\wedge\boldsymbol{v}), \tag{2.1}$$

where $\boldsymbol{v}(\boldsymbol{x}, t)$ is the velocity of the air, $\boldsymbol{\omega} = \nabla\times\boldsymbol{v}$ is the vorticity, and $B = \int \mathrm{d}\bar{p}/\rho(\bar{p}) + \frac{1}{2}v^2$ is the total enthalpy. In the compression wave region ahead of the train, the air may be regarded as linearly perturbed from its mean state, and

$$B \approx \frac{p}{\rho_\mathrm{o}}, \quad \text{where } p = \bar{p} - p_\mathrm{o}. \tag{2.2}$$

According to this model the vorticity $\boldsymbol{\omega}$ vanishes everywhere except within the outer shear layer of the exit flow of the air displaced when the train enters the tunnel. In the absence of the train B is constant throughout the fluid, and it may be assumed that $B = 0$ prior to the arrival of the train.

When the actions of frictional ground forces are ignored during entry into the tunnel, the problem of figure 2(*a*) is dynamically equivalent to calculating the pressure wave generated by the train and the exit-flow vorticity together with their images in the rigid ground plane ($y = 0$) within a duct consisting of the tunnel and its image in the ground (figure 2*b*). This configuration closely resembles the arrangement used in our experiments (§4), and the following discussion is framed in terms of this model.

Let $f \equiv f(x+Ut, y, z) = 0$ be a control surface S contained within the fluid that just encloses the moving train, and suppose that $f < 0$ inside S (in the region occupied by the train) and $f > 0$ in the exterior fluid region. The surface is fixed relative to the train, and the influence of the train on its surroundings can be represented in terms of a collection of monopole and dipole sources distributed on S. The representation is derived by multiplying equation (2.1) by the Heaviside step function $\mathrm{H} \equiv \mathrm{H}(f)$ ($= 0, 1$ according as $f \lessgtr 0$) and rearranging (noting that $\mathrm{D}f/\mathrm{D}t = 0$) to obtain

$$\left(\frac{\mathrm{D}}{\mathrm{D}t}\left(\frac{1}{c^2}\frac{\mathrm{D}}{\mathrm{D}t}\right) - \frac{1}{\rho}\nabla\cdot(\rho\nabla)\right)(\mathrm{H}B) = \frac{1}{\rho}\nabla\cdot(\mathrm{H}\rho\boldsymbol{\omega}\wedge\boldsymbol{v}) - (\nabla B + \boldsymbol{\omega}\wedge\boldsymbol{v})\cdot\nabla\mathrm{H} - \frac{1}{\rho}\nabla\cdot(\rho B\nabla\mathrm{H}). \tag{2.3}$$

This equation is analogous to the differential form of the Ffowcs Williams–Hawkings equation of the theory of aerodynamic sound (Ffowcs Williams & Hawkings 1969);

$\mathrm{H}B \equiv B$ in the fluid ($f > 0$), and the two terms on the right-hand side involving $\nabla\mathrm{H}$ respectively represent monopole and dipole sources distributed over the moving surface $f(x + Ut, y, z) = 0$.

When frictional losses are neglected the momentum equation in the air reduces to $\partial \boldsymbol{v}/\partial t = -\nabla B - \boldsymbol{\omega} \wedge \boldsymbol{v}$. The right-hand side of (2.3) can then be written

$$\frac{\partial}{\partial t}(\boldsymbol{U} \cdot \nabla \mathrm{H}) - \boldsymbol{v} \cdot \nabla \frac{\partial \mathrm{H}}{\partial t} - \frac{1}{\rho}\nabla \cdot (\rho B \nabla \mathrm{H}) + \frac{1}{\rho}\nabla \cdot (\mathrm{H}\rho \boldsymbol{\omega} \wedge \boldsymbol{v}), \tag{2.4}$$

where $\boldsymbol{U} = (-U, 0, 0)$.

The first term in (2.4) is the linear-theory monopole source which was shown by Howe (1998*b*) to account for most of the pressure rise across the compression wavefront. The remaining sources represent effects that are second order in the blockage $\mathscr{A}_\mathrm{o}/\mathscr{A}$. When source terms of order $M(\mathscr{A}_\mathrm{o}/\mathscr{A})^2$ or smaller are neglected, it is permissible to approximate these sources by neglecting the compressibility of the air over S and within the very low Mach number exterior flow from the tunnel portal. If the nonlinear contributions of small changes in density and sound speed to the propagation of the compression wave are also ignored, the general equation (2.3) reduces to

$$\left(\frac{1}{c_\mathrm{o}^2}\frac{\partial^2}{\partial t^2} - \nabla^2\right)(\mathrm{H}B) = \frac{\partial}{\partial t}(\boldsymbol{U} \cdot \nabla \mathrm{H}) + \nabla\cdot(\boldsymbol{v}\, \boldsymbol{U} \cdot \nabla \mathrm{H}) - \nabla\cdot\left\{\left(\frac{p}{\rho_\mathrm{o}} + \tfrac{1}{2}v^2\right)\nabla \mathrm{H}\right\} + \nabla\cdot(\mathrm{H}\boldsymbol{\omega} \wedge \boldsymbol{v}), \tag{2.5}$$

where the relation $\partial \mathrm{H}(f)/\partial t = -\boldsymbol{U} \cdot \nabla \mathrm{H}(f)$ has been used.

2.2. *Linear theory*

When the aspect ratio h/L of the train nose is small the slender body approximation supplies the following representation for the monopole source in (2.5) (Howe 1998*a*, *b*):

$$\frac{\partial}{\partial t}(\boldsymbol{U} \cdot \nabla \mathrm{H})(\boldsymbol{x}, t) \approx \frac{\partial}{\partial t}\left(U\frac{\partial \mathscr{A}_\mathrm{T}}{\partial x}(x + Ut)\,\delta(y)\,\delta(z - z_\mathrm{T})\right). \tag{2.6}$$

In this formula $\mathscr{A}_\mathrm{T}(x)$ is the cross-sectional area of the train at distance x from the tip of the nose, which is assumed to cross the portal entrance plane at $t = 0$. In this approximation the monopole is replaced by a line source distributed at ground level along the centreline of the path of the train: $-\infty < x < \infty$, $y = 0$, $z = z_\mathrm{T}$, where z_T is the offset from the centreline of the tunnel. The source strength is proportional to the rate at which the cross-section changes with distance along the train, and is non-zero only in the vicinity of the train nose (and also the tail).

The corresponding approximation p_1, say, to the compression wave is found by introducing a Green's function $G(\boldsymbol{x}, \boldsymbol{x}', t - \tau)$ which has vanishing normal derivative $\partial G/\partial x_n'$ on the tunnel walls, and satisfies

$$\left(\frac{1}{c_\mathrm{o}^2}\frac{\partial^2}{\partial \tau^2} - \nabla'^2\right) G = \delta(\boldsymbol{x} - \boldsymbol{x}')\,\delta(t - \tau), \quad G = 0 \text{ for } \tau > t, \tag{2.7}$$

where ∇'^2 is the Laplacian with respect to $\boldsymbol{x}'$ (Morse & Feshbach 1953). G can be determined in closed form when the tunnel consists of a semi-infinite, thin-walled, unflanged cylinder of circular cross-section (Howe 1998*a*). In all practical cases, however, the thickness of the compression wavefront is much larger than the tunnel diameter, and $G(\boldsymbol{x}, \boldsymbol{x}'; t - \tau)$ can then be approximated by the compact Green's function. When the observation point $\boldsymbol{x}$ lies within the tunnel ahead of the train this

is given by (Howe 1998*b*)

$$G(\boldsymbol{x},\boldsymbol{x}';t-\tau)\approx\frac{c_\mathrm{o}}{2\mathscr{A}}\left\{\mathrm{H}\left(t-\tau-\frac{|\varphi^*(\boldsymbol{x})-\varphi^*(\boldsymbol{x}')|}{c_\mathrm{o}}\right)-\mathrm{H}\left(t-\tau+\frac{\varphi^*(\boldsymbol{x})+\varphi^*(\boldsymbol{x}')}{c_\mathrm{o}}\right)\right\},\tag{2.8}$$

where $\varphi^*(\boldsymbol{x})$ is the velocity potential of a hypothetical incompressible flow out of the tunnel portal; $\varphi^*(\boldsymbol{x})\sim O(\sqrt{\mathscr{A}})$ in the vicinity of the portal, and is normalized such that

$$\begin{aligned}\varphi^*(\boldsymbol{x})&\approx x-\ell' \quad \text{as } x\to-\infty \text{ inside the tunnel}\\ &\approx -\mathscr{A}/4\pi|\boldsymbol{x}| \quad \text{as } |\boldsymbol{x}|\to\infty \text{ outside the tunnel.}\end{aligned}\tag{2.9}$$

This approximation for G is applicable for any tunnel whose interior cross-sectional area is ultimately constant and equal to $\mathscr{A}$. The length $\ell'\sim\sqrt{\mathscr{A}}$ is an 'end-correction' (Rayleigh 1926) whose value depends on the shape of the tunnel portal. The representation (2.8) is uniformly valid when regarded as a function of either $\boldsymbol{x}$ or $\boldsymbol{x}'$ provided at least one of these points lies within the tunnel at a distance from the portal large compared to the tunnel diameter.

Thus, at points $\boldsymbol{x}$ within the tunnel, ahead of the train where $B=p/\rho_\mathrm{o}$, the linearized approximation $p=p_1$ to the compression wave pressure is given by

$$\begin{aligned}p_1\equiv p_1([t])&=\rho_\mathrm{o}\frac{\partial}{\partial t}\iint_{-\infty}^{\infty}U\frac{\partial\mathscr{A}_\mathrm{T}}{\partial x'}(x'+U\tau)\,G(\boldsymbol{x},x',0,z_\mathrm{T};t-\tau)\mathrm{d}x'\,\mathrm{d}\tau\\ &=\frac{\rho_\mathrm{o}Uc_\mathrm{o}}{2\mathscr{A}}\int_{-\infty}^{\infty}\{\mathscr{A}'_\mathrm{T}(x'-M\varphi^*(x',0,z_\mathrm{T})+U[t]).\\ &\quad -\mathscr{A}'_\mathrm{T}(x'+M\varphi^*(x',0,z_\mathrm{T})+U[t])\}\mathrm{d}x',\end{aligned}\tag{2.10}$$

where the prime on $\mathscr{A}_\mathrm{T}$ denotes differentiation with respect to the argument, and $[t]=t+(x-\ell')/c_\mathrm{o}$ is the effective retarded time. Because nonlinear propagation terms have been ignored, this approximation determines the initial form of the compression wave profile, before the onset of nonlinear steepening. It is therefore applicable within the region several tunnel diameters ahead of the train, during and just after tunnel entry.

The main contributions to the integral (2.10) are from vicinities of the nose and tail of the train, where the cross-sectional area $\mathscr{A}_\mathrm{T}$ is changing. The compression wave is generated as the nose enters the tunnel, and may be calculated by temporarily considering a train of semi-infinite length. During the formation of the wave, and in the particular case in which the Mach number is small enough that terms $\sim O(M^2)$ are negligible, the term $M\varphi^*$ in the arguments of $\mathscr{A}'_\mathrm{T}$ in (2.10) is small, and we then find

$$p_1([t])\approx\frac{\rho_\mathrm{o}U^2}{\mathscr{A}}\int_{-\infty}^{\infty}\frac{\partial\mathscr{A}_\mathrm{T}}{\partial x'}(x'+U[t])\frac{\partial\varphi^*}{\partial x'}(x',0,z_\mathrm{T})\mathrm{d}x',\quad M^2\ll1.\tag{2.11}$$

After the nose has passed into the tunnel, $\partial\varphi^*/\partial x'=1$ in the region occupied by the nose, and (2.11) predicts the overall (linear theory) pressure rise to be $\Delta p_1\approx\rho_\mathrm{o}U^2\mathscr{A}_\mathrm{o}/\mathscr{A}$. But the linear-theory asymptotic pressure rise can also be calculated exactly, with no restriction on Mach number, to be

$$\Delta p_1=\frac{\rho_\mathrm{o}U^2\mathscr{A}_\mathrm{o}}{\mathscr{A}(1-M^2)},\tag{2.12}$$

because this is attained when $\varphi^*(x',0,z_\mathrm{T})\approx x'-\ell'$ in (2.10).

This formula for the overall pressure rise was given by Sugimoto (1994), who approximated the train front by a monopole source but did not consider the details of the compression wave front (see also Howe 1998*c*; Sugimoto & Ogawa 1998). It implies that the approximation (2.11) can be extended to finite Mach numbers by writing

$$p_1([t]) \approx \frac{\rho_o U^2}{\mathscr{A}(1-M^2)} \int_{-\infty}^{\infty} \frac{\partial \mathscr{A}_T}{\partial x'}(x'+U[t]) \frac{\partial \varphi^*}{\partial x'}(x', 0, z_T) \mathrm{d}x'. \tag{2.13}$$

This extrapolation of the linear theory to finite values of M was shown by Howe (1998*c*) to be valid for $M < 0.4$ in the special case of an unflanged, circular cylindrical tunnel. Further justification will be given below in § 3 for flared portals. According to this formula the contribution from the monopole source, which is given exactly by the left-hand side of (2.6), is always $O(\mathscr{A}_o/\mathscr{A})$. This conclusion is not a consequence of the slender-body approximation. Indeed, without making the slender-body approximation it is easily seen that (2.13) remains valid provided only that $\partial\varphi^*/\partial x'$ is replaced by its value *averaged over the periphery of the train at* x', and this average is generally negligibly different from the value of $\partial\varphi^*/\partial x'$ on the axis of the train, except possibly when the track offset z_T is large, and then only at points close to the tunnel portal edge.

Consider a circular cylindrical tunnel of radius R with a flanged entrance (figure 2*b*), and a train with an ellipsoidal nose profile obtained by rotating the curve $y = h\sqrt{(x/L)(2-x/L)}$, $0 < x < L$ about the x-axis, so that

$$\frac{\mathscr{A}_T(x)}{\mathscr{A}_o} = \begin{cases} (x/L)(2-(x/L)), & 0 < x < L \\ 1, & x > L, \end{cases} \tag{2.14}$$

where $\mathscr{A}_o = \pi h^2$. This axisymmetric model is used in our experiments described in § 4, with

$$h = 2.235\,\mathrm{cm}, \quad L = 11.18\,\mathrm{cm}. \tag{2.15}$$

The tail of the model train has an identical ellipsoidal shape, and the overall length of the train is 91.5 cm. The tunnel radius $R = 5$ cm (so that the blockage $\mathscr{A}_o/\mathscr{A} \approx 0.2$), the overall tunnel length is 10 m, and pressure measurements are made at a distance $|x| = 1$ m from the tunnel entrance. The potential function $\varphi^*(\boldsymbol{x})$ is easily computed using a finite difference or boundary element integration scheme for Laplace's equation, and may be assumed to be known for the given tunnel geometry.

The measurements described in § 4 are for the simplest configuration in which the tunnel and train are coaxial, so that $z_T = 0$ in (2.13). The curve labelled p_1 in figure 3 is the linear theory representation of the wavefront pressure profile calculated from (2.13), (2.14) for $U = 293$ k.p.h. ($M = 0.24$), plotted against the non-dimensional retarded position of the train $U[t]/R$ (the nose of the train being assumed to enter the tunnel at $t = 0$). The open triangles are measured values of the pressure. The initial pressure rise occurs over a time interval $\sim 2R/U$, corresponding to a wavefront thickness $2R/M \sim 41$ cm. The rapid decrease in the measured pressure that occurs for $U[t]/R > 14$ is produced by the rarefaction wave generated when the tail enters the tunnel. The gradual increase in the experimental points after $U[t]/R \sim 2$ is believed to be caused by boundary layer growth on the train and tunnel walls, or possibly by flow separation on either of these surfaces, and is discussed further in § 2.4.

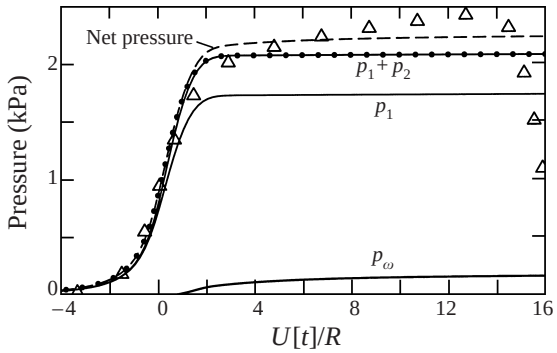

FIGURE 3. Illustrating different approximations for the compression wave pressure profile (in kPa) for a train with the ellipsoidal nose profile (2.14) entering a flanged circular cylindrical tunnel of radius $R = 5\,\mathrm{cm}$ at $U = 293\,\mathrm{k.p.h.}$: the solid curves depict the linear theory pressure p_1 (equation (2.13)), the second-order approximation $p_1 + p_2$ of equation (2.20), and the exit-flow vorticity-generated pressure p_ω (equation (2.25)); • • •, the simplified second-order approximation (2.22); - - - -, the net predicted pressure $p_1 + p_2 + p_\omega$ calculated from (2.22) and (2.25); △ △ △, the measured pressure at a distance of 1 m from the tunnel entrance plane (§ 4).

2.3. *The contributions from the surface dipoles*

The second and third terms on the right of (2.5) are dipole sources distributed over the surface of the train. In the slender-body approximation the first of these becomes

$$\nabla\cdot(\boldsymbol{v}\,\boldsymbol{U}\cdot\nabla\mathrm{H}) \approx \frac{\partial}{\partial x}\left(u_x U\frac{\partial \mathscr{A}_\mathrm{T}}{\partial x}(x+Ut)\,\delta(y)\,\delta(z-z_\mathrm{T})\right), \tag{2.16}$$

where u_x is the x-component of the air velocity $\boldsymbol{v}$. The strength of the second dipole is proportional to $p/\rho_\mathrm{o} + \frac{1}{2}v^2$. This can be estimated by means of a quasi-static approximation, using Bernoulli's equation and the linear-theory uniform pressure $p_1(t)$ just ahead of the train, to be given by

$$\frac{p}{\rho_\mathrm{o}} + \tfrac{1}{2}v^2 \approx \frac{p_1(t)}{\rho_\mathrm{o}} - u_x U, \tag{2.17}$$

so that in the slender-body approximation

$$-\nabla\cdot\left\{\left(\frac{p}{\rho_\mathrm{o}} + \tfrac{1}{2}v^2\right)\nabla\mathrm{H}\right\} \approx \frac{\partial}{\partial x}\left\{\left(\frac{p_1(t)}{\rho_\mathrm{o}} - u_x U\right)\frac{\partial \mathscr{A}_\mathrm{T}}{\partial x}(x+Ut)\,\delta(y)\,\delta(z-z_\mathrm{T})\right\}. \tag{2.18}$$

Combining (2.16) and (2.18), we obtain the

$$\text{net surface dipole} \approx \frac{\partial}{\partial x}\left(\frac{p_1(t)}{\rho_\mathrm{o}}\frac{\partial \mathscr{A}_\mathrm{T}}{\partial x}(x+Ut)\,\delta(y)\,\delta(z-z_\mathrm{T})\right). \tag{2.19}$$

Hence, using the Green's function (2.8) and neglecting terms of order $M(\mathscr{A}_\mathrm{o}/\mathscr{A})^2$ and smaller, the surface dipole contribution p_2, say, to the compression wave pressure is found to be given by

$$p_2 \equiv p_2([t]) \approx \frac{p_1([t])}{\mathscr{A}}\int_{-\infty}^{\infty}\frac{\partial \mathscr{A}_\mathrm{T}}{\partial x'}(x'+U[t])\frac{\partial \varphi^*}{\partial x'}(x',0,z_\mathrm{T})\mathrm{d}x'. \tag{2.20}$$

This yields a component of order $\rho_\mathrm{o}U^2(\mathscr{A}_\mathrm{o}/\mathscr{A})^2$ to the overall pressure rise Δp across the compression wavefront.

The solid curve labelled $p_1 + p_2$ in figure 3 is the second-order approximation $p = p_1 + p_2$ for the experimental conditions of § 2.2, which exhibits a considerably improved agreement with experiment relative to the approximation p_1. A further simplification can be introduced by noting that p_2 is initially very small, which suggests that the integral in (2.20) may be approximated by its value for large retarded time (when $\partial\varphi^*/\partial x' = 1$), and therefore that

$$p_2 \approx p_1 \frac{\mathscr{A}_o}{\mathscr{A}}. \tag{2.21}$$

The corresponding prediction of $p_1 + p_2$ across the wavefront is shown by the dotted curve in figure 3. The difference between the two approximations for $p_1 + p_2$ is insignificant, and the overall pressure wave produced by the monopole and dipole source terms is therefore represented well by

$$p = p_1 + p_2 \approx \frac{\rho_o U^2}{\mathscr{A}(1-M^2)} \left(1 + \frac{\mathscr{A}_o}{\mathscr{A}}\right) \int_{-\infty}^{\infty} \frac{\partial \mathscr{A}_T}{\partial x'}(x' + U[t]) \frac{\partial \varphi^*}{\partial x'}(x', 0, z_T) \mathrm{d}x'. \tag{2.22}$$

2.4. *Contribution from the exit-flow vorticity*

When boundary layer growth on the train and on the interior tunnel walls is ignored, the vorticity source $\nabla\cdot(\mathrm{H}\boldsymbol{\omega} \wedge \boldsymbol{v})$ in equation (2.5) is non-zero only in the shear layer of the exit flow from the tunnel (see figure 2). Observations indicate that the exit-flow shear layer rolls-up and forms a large vortex (Auvity & Bellenoue 1998) that will be essentially axisymmetric when the train travels along the tunnel centreline. Just after tunnel entry the initial stages of vortex formation may be modelled as in figure 2, where in the simplest approximation the exit flow is assumed to be a uniform jet with speed $u_E(t)$, with vorticity confined to a circular cylindrical vortex sheet of strength u_E convecting in the positive x-direction at speed $\frac{1}{2}u_E$, so that

$$\nabla\cdot(\mathrm{H}\boldsymbol{\omega} \wedge \boldsymbol{v}) = \begin{cases} (R/r)(\partial/\partial r)\left(\frac{1}{2}u_E^2 \delta(r-R)\right), & 0 < x < s(t) \\ 0, & \text{elsewhere,} \end{cases} \tag{2.23}$$

where $s(t)$ is the length of the jet outside the portal, indicated in figure 2(b), and $r = \sqrt{y^2 + z^2}$ is radial distance from the tunnel axis.

The velocity $u_E(t)$ increases rapidly from zero to its final value of $U\mathscr{A}_o/\mathscr{A}$ during the time $\sim L/U$ in which the nose enters the tunnel. The initial growth of the vortex source strength will be modelled by setting $u_E(t) = U\mathscr{A}_T(Ut)/\mathscr{A}$ for $0 < t < L/U$. The corresponding growth of the vortex-generated pressure wave depends on both $u_E(t)$ and $s(t)$; the latter may be approximated by $s(t) = \int_0^t u_E(\tau)\mathrm{d}\tau$, $t > 0$. Using Green's function (2.8), the pressure p_ω generated by the exit flow may then be cast in the form

$$p_\omega([t]) \approx \frac{\rho_o U^2}{2\mathscr{A}} \left(\frac{\mathscr{A}_T(U[t])}{\mathscr{A}}\right)^2 \int_0^{s([t])} 2\pi R \left(\frac{\partial \varphi^*}{\partial r'}\right)_{r'=R} \mathrm{d}x'. \tag{2.24}$$

The integral is equal to the flux through the boundary of the jet (of length s) of the hypothetical irrotational flow from the tunnel portal defined by the velocity potential φ^*. It can therefore be evaluated explicitly in terms of the corresponding Stokes stream function $\psi^*(r', x')$ (Lamb 1932) which satisfies

$$\frac{1}{r'}\frac{\partial \psi^*}{\partial r'} = \frac{\partial \varphi^*}{\partial x'}, \quad \frac{1}{r'}\frac{\partial \psi^*}{\partial x'} = -\frac{\partial \varphi^*}{\partial r'}.$$

On the jet boundary ($r' = R$) $\psi^*(R, x')$ decreases from $\mathscr{A}/2\pi$ at $x' = 0$ to zero at

$x' = +\infty$, and we find

$$p_\omega([t]) \approx \frac{\rho_o U^2}{2}\left(\frac{\mathscr{A}_T(U[t])}{\mathscr{A}}\right)^2\left(1 - \frac{2\pi\psi^*(R, s([t]))}{\mathscr{A}}\right). \tag{2.25}$$

The same numerical calculation that must be performed to determine the potential φ^* also yields the Stokes stream function ψ^*, thereby permitting straightforward evaluation of the right-hand side of (2.25). The magnitude of p_ω is of the same order as the surface dipole pressure p_2; its growth as the train enters the tunnel is shown in figure 3 for the experimental conditions of § 2.2.

The broken line curve in figure 3 represents the predicted overall pressure signature from all three sources:

$$p = p_1 + p_2 + p_\omega. \tag{2.26}$$

The gradual increase in p_ω as the exit flow extends downstream causes p to continue to increase (but very slowly) after the establishment of the main compression wavefront. The predicted growth rate is smaller than that of the measured pressure, presumably because of the neglect of vorticity sources in the viscous boundary layers on the train and tunnel walls, and within any regions of separated flow.

2.5. *Comparison with Hara's gas dynamic formula for* Δp

Hara (1961) has developed a comprehensive formula for the overall pressure rise Δp across the compression wavefront in a cylindrical tunnel based on the general equations of steady-flow gas dynamics. When the air flow is assumed to be homentropic, and when the exit flow from the portal is modelled by a semi-infinite uniform jet, bounded by a cylindrical vortex sheet (as in figure 2), he finds

$$\Delta p = \frac{\rho_o U^2}{(1-M^2)}\frac{\mathscr{A}_o}{\mathscr{A}}\frac{\left(1 - \dfrac{\mathscr{A}_o}{2\mathscr{A}}\right)}{\left[1 - \dfrac{2}{(1+M)}\dfrac{\mathscr{A}_o}{\mathscr{A}}\left(1 - \dfrac{\mathscr{A}_o}{2\mathscr{A}}\right)\right]} \tag{2.27}$$

$$\approx \frac{\rho_o U^2}{(1-M^2)}\frac{\mathscr{A}_o}{\mathscr{A}}\left(1 + \frac{3}{2}\frac{\mathscr{A}_o}{\mathscr{A}} + \cdots\right), \tag{2.28}$$

where in (2.28) small terms of order $M\mathscr{A}_o/\mathscr{A}$ and $(\mathscr{A}_o/\mathscr{A})^2$ relative to unity have been discarded. The solid curves in figure 4 represent the prediction (2.27) of Δp (kPa) plotted as a function of the blockage $\mathscr{A}_o/\mathscr{A}$ for train Mach numbers M varying from 0.1 to 0.4.

Δp can also be calculated to the same order as (2.28) from equations (2.22) and (2.25). When $U[t]/R \gg 1$ equation (2.22) supplies (with $\partial\varphi^*/\partial x' \equiv 1$) the second-order prediction

$$\Delta p_1 + \Delta p_2 = \frac{\rho_o U^2}{(1-M^2)}\frac{\mathscr{A}_o}{\mathscr{A}}\left(1 + \frac{\mathscr{A}_o}{\mathscr{A}}\right). \tag{2.29}$$

In the same limit $\psi^*(R, s([t])) \to 0$, and equation (2.25) gives

$$\Delta p_\omega = \frac{\rho_o U^2}{2}\left(\frac{\mathscr{A}_o}{\mathscr{A}}\right)^2 \approx \frac{\rho_o U^2}{(1-M^2)}\frac{1}{2}\left(\frac{\mathscr{A}_o}{\mathscr{A}}\right)^2, \quad M^2\left(\frac{\mathscr{A}_o}{\mathscr{A}}\right) \ll 1. \tag{2.30}$$

Hence, $\Delta p_1 + \Delta p_2 + \Delta p_\omega$ coincides with the approximation (2.28) of Hara's formula. However, according to figure 3 the asymptotic contribution Δp_ω to the overall pressure

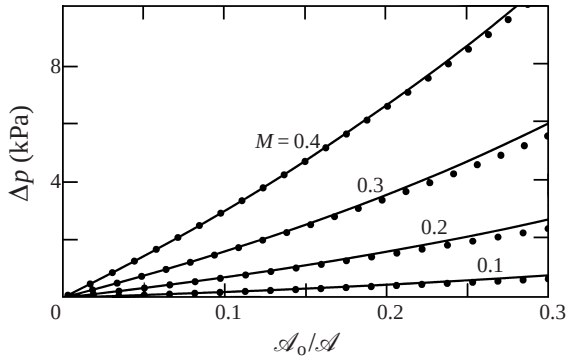

FIGURE 4. Comparison of the overall pressure rise Δp predicted by the Hara formula (2.27) (——) and the second-order, surface source approximation $\Delta p_1 + \Delta p_2$ given by (2.29) (• • •).

rise is not attained until well after the formation of the compression wavefront, at times when predictions of Hara's irrotational tunnel-flow theory are likely to be contaminated by separation or by boundary layer growth on the train and tunnel walls. In practice, therefore, the second-order approximation (2.29) probably gives a better indication of the initial pressure rise across the wavefront. This is plotted as the dotted curves in figure 4; predictions of the two theories agree for $\mathscr{A}_o/\mathscr{A} < 0.22$.

3. The Flared Portal

Turn attention now to the case of a train entering a flanged tunnel of semi-circular cross-section that is flared over an axial distance ℓ from the tunnel entrance plane (figure 5*a*). Measurements described in §4 are made for this configuration using the axisymmetric model of figure 5(*b*), to which the following discussion is confined.

3.1. *The function* φ^*

Let the tunnel cross-sectional area $S(x)$ decrease smoothly from $\mathscr{A}_E \equiv \pi R_E^2$ at $x = 0$ to the uniform, constant value $\mathscr{A} = \pi R^2$ for $x \leqslant -\ell$. Changes in $S(x)$ are assumed to be sufficiently slow that the velocity potential φ^* satisfies the following simplified form of Laplace's equation within the tunnel (Howe 1999*b*):

$$\frac{1}{S(x)}\frac{\partial}{\partial x}\left(S(x)\frac{\partial \varphi^*}{\partial x}\right) = 0, \quad x < 0, \tag{3.1}$$

with solution

$$\varphi^*(\boldsymbol{x}) = \mathscr{A}\int_0^x \frac{\mathrm{d}\xi}{S(\xi)} + C, \quad x < 0, \tag{3.2}$$

where C is a constant.

If the flange is regarded as infinite, the behaviour of $\varphi^*(\boldsymbol{x})$ outside the tunnel ($x > 0$) is approximately the same as the potential of incompressible flow produced by a 'piston' of area $\mathscr{A}_E$ in a plane wall at $x = 0$, moving with normal velocity $\left(\partial\varphi^*/\partial x\right)_{x=0} = \mathscr{A}/\mathscr{A}_E$. When $\boldsymbol{x}$ lies on the axis of symmetry (the x-axis), the condition that $\varphi^*(\boldsymbol{x}) \to 0$ as $x \to +\infty$ then yields (for details see Howe 1999*b*)

$$\varphi^*(\boldsymbol{x}) = -\frac{\mathscr{A}R}{\mathscr{A}_E}\left[\left(\frac{\mathscr{A}_E}{\mathscr{A}} + \frac{x^2}{R^2}\right)^{1/2} - \frac{x}{R}\right], \quad x > 0. \tag{3.3}$$

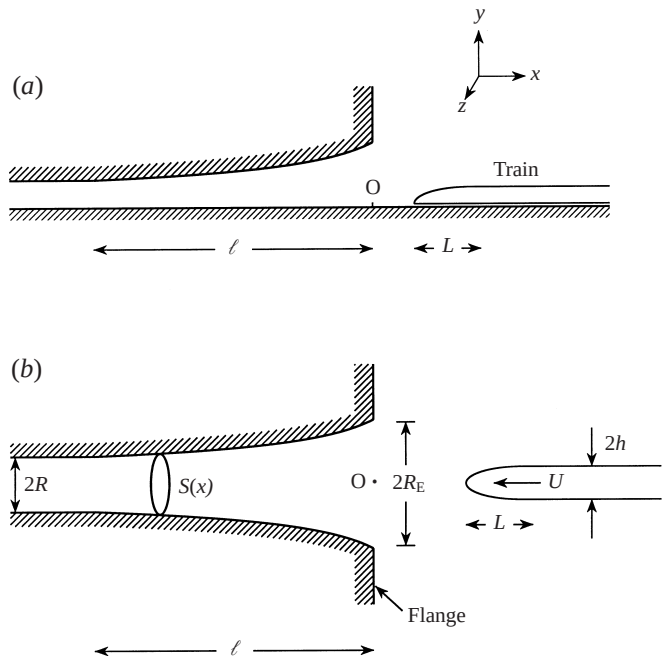

FIGURE 5. (*a*) Train entering a tunnel with a flared portal of length ℓ; (*b*) axisymmetric flared portal with an infinite flange.

Equating expressions (3.2) and (3.3) at $x = 0$ we find $C = -R\sqrt{\mathscr{A}/\mathscr{A}_E}$, and the flared portal 'end correction' is then given by

$$\ell' = R\sqrt{\frac{\mathscr{A}}{\mathscr{A}_E}} + \int_{-\infty}^{0} \left(\frac{\mathscr{A}}{S(\xi)} - 1\right) \mathrm{d}\xi. \tag{3.4}$$

3.2. *Optimal flaring*

The flaring is 'optimal' when the pressure increases linearly with distance across the compression wavefront. Howe (1999*b*) derived the shape of the tunnel area profile $S(x)$ necessary to achieve this by considering the linear-theory compression wave p_1 produced by a monopole point source entering the tunnel. Equation (2.13) reveals that this is equivalent to setting

$$\frac{\partial \mathscr{A}_T}{\partial x'}(x' + U[t]) = \mathscr{A}_o \delta(x' + U[t]), \tag{3.5}$$

i.e. to replacing the streamlined train nose profile by a flat-faced or 'snub-nosed' train.

However, because the second-order approximation (2.22) for $p_1 + p_2$ differs from the linear-theory pressure (2.13) merely by a multiplicative factor of $(1 + \mathscr{A}_o/\mathscr{A})$, the linear-theory optimal tunnel profile remains optimal at second order. Indeed, substituting from (3.2) and (3.5) into (2.22), we find that

$$p \approx p_1 + p_2 = \frac{\rho_o U^2}{(1 - M^2)} \left(1 + \frac{\mathscr{A}_o}{\mathscr{A}}\right) \frac{\mathscr{A}_o}{S(-U[t])} \quad \text{for } U[t]/R > 0, \tag{3.6}$$

after the point source has crossed the entrance plane into the flared section of the tunnel, where most of the pressure rise occurs. During this time $S(-U[t])$ decreases

from $\mathscr{A}_E$ to $\mathscr{A}$, and the pressure rises from

$$\frac{\rho_o U^2}{(1-M^2)}\left(1+\frac{\mathscr{A}_o}{\mathscr{A}}\right)\frac{\mathscr{A}_o}{\mathscr{A}_E}$$

at the instant at which the front of the train (the source) enters the tunnel, to its final value of

$$\frac{\rho_o U^2}{(1-M^2)}\left(1+\frac{\mathscr{A}_o}{\mathscr{A}}\right)\frac{\mathscr{A}_o}{\mathscr{A}}$$

when the front enters the uniform section of the tunnel. This increase will be linear when $1/S(-U[t])$ is a linearly increasing function of the retarded time, that is, when the flared section of the tunnel is defined by

$$\frac{S(x)}{\mathscr{A}} = 1\Big/\left[\frac{\mathscr{A}}{\mathscr{A}_E}-\frac{x}{\ell}\left(1-\frac{\mathscr{A}}{\mathscr{A}_E}\right)\right], \quad -\ell < x < 0. \tag{3.7}$$

It remains to specify the cross-sectional area $S(0) = \mathscr{A}_E$ in the tunnel entrance plane. When the length ℓ of the flared section is prescribed, the value of $\mathscr{A}_E$ must be adjusted to ensure that the pressure varies smoothly at $U[t]/R = 0$, when the train (source) enters the tunnel. This is done by requiring the values of $\partial^2\varphi^*(x,0,0)/\partial x^2$ defined respectively by the approximations (3.2) and (3.3) to be equal at $x = 0$, which implies that

$$\left(\frac{\mathscr{A}}{\mathscr{A}_E}\right)^{3/2} = \frac{R}{\ell}\left(1-\frac{\mathscr{A}}{\mathscr{A}_E}\right).$$

Provided that the length ℓ of the flared section exceeds $2R/3\sqrt{3} \approx 0.385R$, we then find

$$\frac{\mathscr{A}_E}{\mathscr{A}} = \left(\frac{\ell}{2R}\right)^{2/3}\left[\left(1+\sqrt{1-\left(\frac{2R}{3\sqrt{3}\ell}\right)^2}\right)^{1/3}+\left(1-\sqrt{1-\left(\frac{2R}{3\sqrt{3}\ell}\right)^2}\right)^{1/3}\right]^2. \tag{3.8}$$

This gives a minimum value of $\mathscr{A}_E/\mathscr{A} = \frac{4}{3}$ at $\ell/R = 0.385$; when $\ell \gg R$, $\mathscr{A}_E/\mathscr{A} \approx (\ell/R)^{2/3}$. In our experiments $\ell/R = 10$, so that the optimal area ratio $\mathscr{A}_E/\mathscr{A} = 5.35$ and $R_E/R = 2.31$. The local tunnel radius is given by $r(x) = R\sqrt{S(x)/\mathscr{A}}$, and the flared sections shown in figure 5 are the optimal profile calculated from this formula and equations (3.7), (3.8) when $\ell/R = 10$.

3.3. *Comparison with measurements*

Numerical results discussed by Howe (1999*b*) indicated that the linear-theory pressure p_1 continues to increase linearly across the wavefront when the 'snub'-nosed train is replaced by one of more realistic profile. This is because the linear-theory monopole distribution (2.6) can be replaced to a good approximation by a point source at a suitable 'centroid' within the nose of the train. In figure 6 the linear-theory pressure p_1, determined by (2.13), (3.1) and (3.3), and the second-order approximation p_1+p_2 given by (2.22), (3.1) and (3.3), are compared with measurements for the circular cylindrical tunnel of § 2.2 fitted with a flanged portal that is optimally flared in accordance with equations (3.7), (3.8) with

$$R = 5\,\text{cm}, \quad \ell = 10R.$$

The open triangles are the pressure measured at distance 1.55 m from the portal entrance plane produced by an axisymmetric train of total length 91.5 cm. The train is the same as that described in § 2.2, both ends of which have ellipsoidal profiles

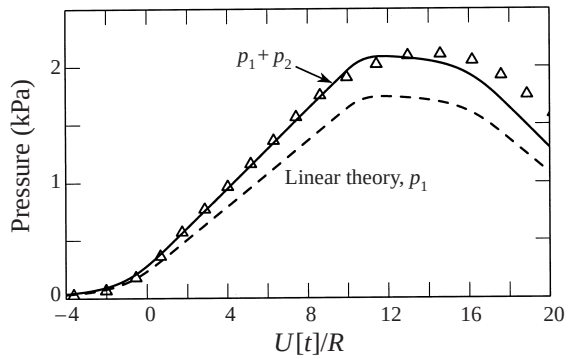

FIGURE 6. Compression wave pressure profile (in kPa) generated by a train with ellipsoidal nose and tail profiles defined by (2.14) entering at $U = 296$ k.p.h. a circular cylindrical tunnel of radius $R = 5$ cm with an optimally flared portal of length $\ell = 50$ cm: △ △ △, pressure measured at a distance 1.55 m from the tunnel entrance plane; - - - -, linear theory pressure predicted by (2.13), (3.2), (3.3); ——, second-order approximation $p_1 + p_2$ given by (2.22), (3.2), (3.3).

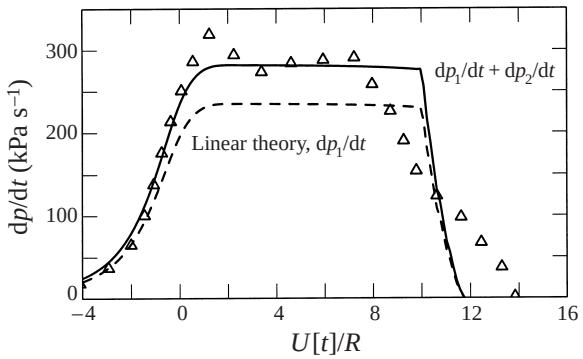

FIGURE 7. Compression wave 'pressure gradient' dp/dt (in kPa s^{-1}) generated by a train with ellipsoidal nose and tail profiles defined by (2.14) entering at $U = 296$ k.p.h. a circular cylindrical tunnel of radius $R = 5$ cm with an optimally flared portal of length $\ell = 50$ cm: △ △ △, pressure gradient measured at a distance 1.55 m from the tunnel entrance plane; - - - -, linear theory prediction of (2.13), (3.2), (3.3); ——, second-order approximation $dp_1/dt + dp_2/dt$ determined by (2.22), (3.2), (3.3).

defined as in (2.14) with semi-axes h, L given by (2.15), the blockage $\mathscr{A}_o/\mathscr{A} = 0.2$, and the train speed $U = 296$ k.p.h.

The nose of the train enters the flared section of the tunnel at $U[t]/R = 0$, following which the pressure rises linearly until just after the nose arrives at the beginning of the uniform section of the tunnel, at $U[t]/R = 10$, so that the compression wave thickness $\sim 10R/M = 207$ cm (representing a fivefold increase over the wave thickness in § 2 for the flanged, circular cylindrical portal). The second-order approximation (2.22) gives an excellent rendering of this experimental observation. The subsequent sharp decrease in the pressure is produced by the expansion wave generated when the tail of the train begins to enter the flared section at $U[t]/R \approx 16$. Because of the large expansion in cross-section of the tunnel at the portal, the contribution p_ω to the pressure rise from the exit flow vorticity is reduced by a factor $(\mathscr{A}/\mathscr{A}_E)^2 \sim 0.035$, and may be ignored.

Measured and predicted values of the temporal 'pressure gradient' dp/dt are

compared in figure 7. The value of $\mathrm{d}p/\mathrm{d}t$ (augmented by nonlinear steepening) governs the strength of the micro-pressure wave radiated from the far end of the tunnel when the compression wave arrives. The initial maximum value of about $310\,\mathrm{kPa\,s^{-1}}$ shown in figure 7 is about 25% of the corresponding maximum for the pressure profile of figure 3 for the unflared circular cylindrical tunnel. The abrupt decrease in the predicted pressure gradient at $U[t]/R = 10$ occurs as the nose of the train enters the uniform section of the tunnel. The measured decrease of $\mathrm{d}p/\mathrm{d}t$ at these times is much smoother, presumably because various vortex sources discussed above are ignored in the theory; in particular these could well include a large vortex-ring-like structure between the train and tunnel wall in the flared section, although no experimental data are currently available to support this conjecture.

Measurements of the compression wave and pressure gradient for an unflanged entrance with the same flared portal (that, strictly speaking, is 'optimal' only in the presence of a flange) show a similar linear growth in pressure across the compression wavefront occurring during the passage of the nose across the flared section, and an overall minimum value of $\mathrm{d}p/\mathrm{d}t$ that agrees with the 'flanged' theory based on the approximations (3.7), (3.8). According to equation (3.6), the flange only affects the growth of the compression wave at times prior to the entrance of the 'centroid' of the nose into the flared section, and in the optimal case it has a negligible influence on the dynamics of the compression wave formation, so that predictions for the optimal portal are valid for both the flanged and unflanged tunnels.

4. Description of the model scale experiments

4.1. *Experimental apparatus*

The Reynolds number of the dominant air flow induced by a high-speed train is sufficiently large that the aerodynamics of a train entering a tunnel may be regarded as inviscid. To a good approximation, therefore, the compression wave characteristics scale on Mach number and blockage, so that measurements at model scale will provide a faithful representation of full scale results provided the Mach number and relative geometrical sizes of the tunnel and train are the same (Ozawa *et al.* 1976; Ozawa & Maeda 1988). In our experiments the uniform section of the tunnel has a circular cross-section of radius $R = 5\,\mathrm{cm}$. The areas of tunnels on the Japanese high-speed *Shinkansen* network are typically about $63\,\mathrm{m^2}$. When this is doubled to take account of the image tunnel in the ground plane, the equivalent circular cylindrical tunnel has radius 6.35 m, which means that the experiments reported here are 1/127 of full scale.

The experiments were performed at the Railway Technical Research Institute in Tokyo using the apparatus illustrated schematically in figure 8. The uniform section of the tunnel consists of a 10 m long horizontal, circular cylindrical pipe made of vinyl chloride, with inner and outer diameters respectively equal to 10 cm and 11.4 cm. Axisymmetric model trains are projected at high speed into the tunnel, guided by a 5 mm diameter taut steel wire extending along the tunnel axis. Both flanged and unflanged tunnel entrance portals are used. The outer contour of the flange is a square of side 1 m, which is larger by a factor of 10 than the inner diameter of the uniform section of the tunnel. The tunnel entrance can be fitted with a (flanged or unflanged) flared portal, which increases the overall tunnel length by 55 cm. The photograph in figure 9 shows the experimental arrangement for an unflanged, flared portal.

The overall length of the experimental apparatus shown in figure 8 is about 18 m.

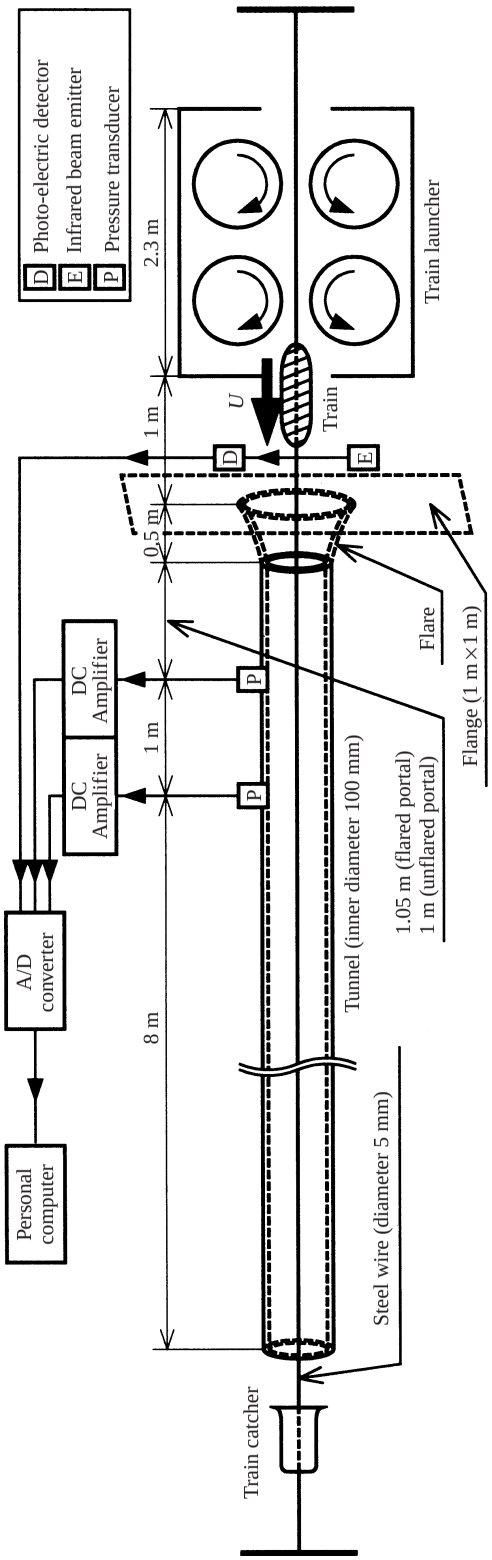

FIGURE 8. Schematic of the experimental apparatus.

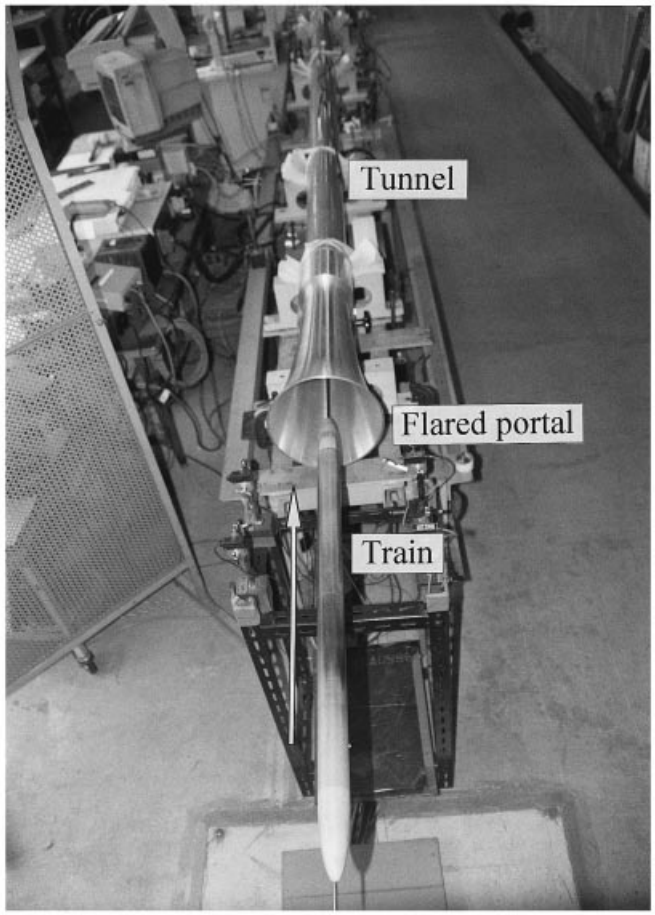

FIGURE 9. Unflanged flared portal and cylindrical tunnel with wire-guided axisymmetric model train.

The train is launched by a two-stage friction drive consisting of two pairs of vertically aligned wheels. It is accelerated to about 200 k.p.h. by the first stage and then to a maximum speed of about 320 k.p.h. by the second, the final speed being controlled by varying the rates of rotation of the wheels. A 1 m long 'open' section between the launcher and the flared portal is large enough to ensure that pressure waves generated during the rapid acceleration of the train are negligible at the tunnel entrance. On emerging from the far end of the tunnel, the train is brought to rest by a 'catcher' that slides along the steel wire, the motion being damped by a cloth and sponge shock-absorber fixed to the wall supporting the end of the wire. The catcher contains an air damper and fabric material to absorb the kinetic energy of the rapidly decelerating train, which is recovered without damage and can be used repeatedly in further tests.

Pressure measurements are made within the tunnel using two wall-mounted transducers respectively at 1 and 2 m from the start of the uniform, circular cylindrical tunnel. The pressures are recorded until the instant at which the expansion wave produced by reflection of the compression wave at the far tunnel exit is received by the second transducer. This occurs about 45 ms after the nose of the train enters the flared portal, which is well in excess of the 10 ms required for recording the wavefront

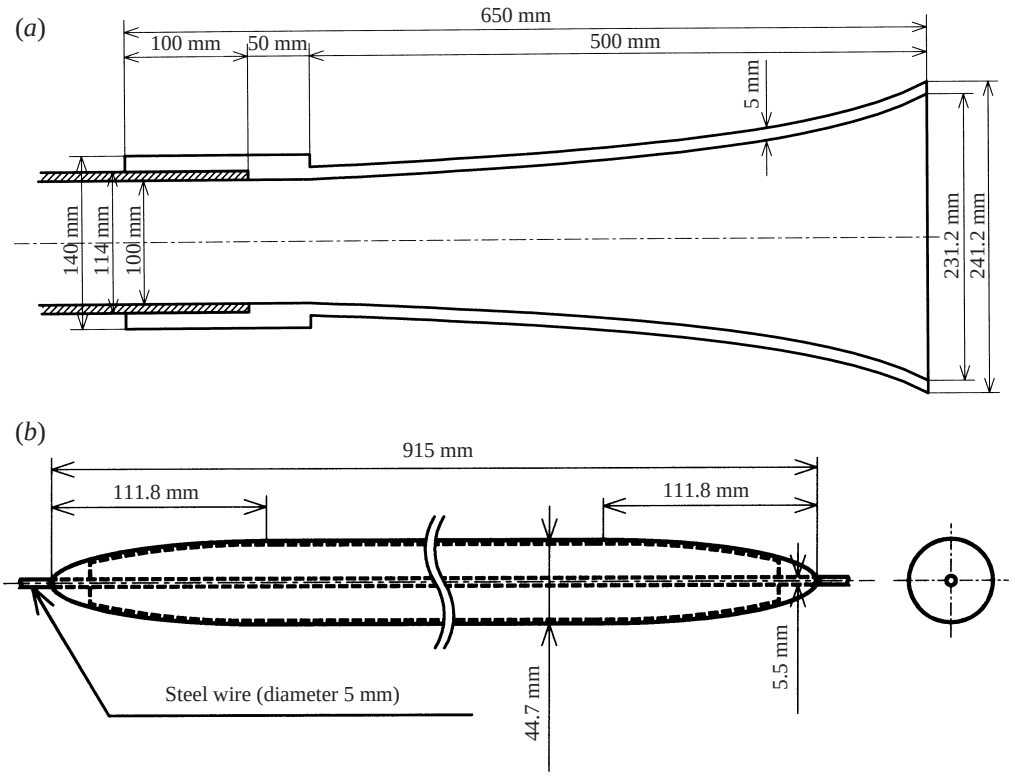

FIGURE 10. (*a*) The optimally flared portal fitted to the end of the circular cylindrical tunnel. (*b*) Model train with ellipsoidal nose and tail.

of the compression wave generated by a train entering the flared portal at about 300 k.p.h.

The dimensions of the 'optimally' flared portal are given in figure 10(*a*). The portal is fabricated from 5 mm thick aluminium alloy; a 10 cm collar at its narrow end permits it to mate smoothly with the uniform, circular cylindrical section of the tunnel. When fitted to the cylinder, the portal has an overall length of 55 cm, and a 'working length' of $\ell = 50$ cm measured from the tunnel inlet plane, within which the cross-sectional area $S(x)$ varies according to equations (3.7), (3.8).

The model train (figure 10*b*) consists of an axisymmetric, cigar-shaped body of length 91.5 cm with rounded ellipsoidal ends, defined as in (2.14) with $L = 11.18$ cm and radius $h = 2.235$ cm; it is made from a nylon plastic material of total mass 660 g. The steel guide-wire passes axisymmetrically through a cylindrical hole in the model of diameter 5.5 mm. For these dimensions the blockage $\mathscr{A}_0/\mathscr{A} = 0.2$ (or 0.198 if account is taken of the cross-sectional area of the guide-wire), which is typical of the larger values arising in practice, where for high-speed operations ($U > 200$ k.p.h.) $\mathscr{A}_0/\mathscr{A}$ is usually restricted to the range 0.12 to 0.22.

4.2. *Measurement of the compression wave*

An infrared beam directed across the open section in front of the tunnel entrance is used to detect the entrance of the train nose into the tunnel. Pressure measurements are automatically initiated when the beam is cut. The total time for which the beam is cut can also be used to estimate the speed U of the train, but this method is subject

to large errors because of possible lateral vibrations of the guide wire, and a more accurate procedure described below in § 4.3 was therefore used.

The pressure within the tunnel was measured by two *Toyoda Machine Works PD104K* transducers mounted in the tunnel wall at distances of 1.55 m and 2.55 m from the entrance plane of the flared portal, and at distances of 1 m and 2 m from the entrance plane in the case of the uniform, circular cylindrical tunnel. Data from the transducers are passed through a *Toyoda Machine Works AA6210* amplifier, digitized using a 12-bit analogue-to-digital converter with a sampling rate of 25 kHz per channel, and stored in a personal computer. The pressure gradient ($\mathrm{d}p/\mathrm{d}t$) is then calculated using a simple central difference scheme after high-frequency components (> 1 kHz) of the measured pressure have been removed using a fast Fourier transform algorithm.

4.3. *Measurement of U*

The pressure gradient $\mathrm{d}p/\mathrm{d}t$ varies approximately as the third power of the train speed, so that a proper comparison of theory and experiment requires careful measurement of U. High-speed photography indicates that lateral vibrations of the model train on the guide wire often occur at amplitudes as large as 5 mm as the train enters the tunnel. Because of the rounded train nose and tail profiles, it is likely that measurements of U based on observations of the time interval during which the infrared beam is blocked by the train can be as large as 2.5%, giving a possible error of about 8 k.p.h. when $U \sim 300$ k.p.h.

We therefore adopted a measurement technique based on observations of the hydrodynamic field of the tail of the train within the tunnel. The air motion relative to the tail is essentially steady during the time interval following its entry into the uniform section of the tunnel until the first arrival at the tail of waves reflected from the far end of the tunnel. For the present series of experiments this interval includes the times during which the tail passes the two pressure transducers, and measurements of the time lapse between respective observations by the transducers of identical pressure signatures can therefore be used to determine U. Of course, a rarefaction wave is generated when the tail enters the tunnel, and this is partially reflected at the front of the train and could in principle disturb the hydrodynamic flow at the tail. However, the blockage $\mathscr{A}_0/\mathscr{A} = 0.2$ is small enough that the amplitude of the reflected wave turns out to be negligible. Similarly, flow separation near the tail of the present model train is sufficiently small scale to produce no significant unsteady pressures. Thus, pressure measurements at the two locations yield no distinguishable differences between the corresponding pressure signatures of the tail. The accuracy of this procedure is further improved by comparing the signatures of $\mathrm{d}p/\mathrm{d}t$ rather than p, in which case the measurement error is estimated to be no more than about 0.5% (1.5 k.p.h.) when $U \sim 300$ k.p.h.

Lateral vibrations of the train on the steel wire are a possible source of unsteadiness that can also affect the accuracy of this measurement. The natural frequency of these vibrations was estimated by hitting the steel wire when the train is stationary, and turns out to be about 11 Hz. When $U \sim 300$ k.p.h., the train travels about 7.5 m during one period when the lateral motion is, say, 5 mm. The lateral motion of the train over the 1 m distance between the pressure transducers is therefore less than 1 mm, and is hardly likely to modify significantly the near-field pressure fluctuations. Similarly, by using a system of four pressure transducers to measure the train speed at different positions within the tunnel (in the range 250–300 k.p.h.), it was concluded that uncertainties in the measured speed attributable to a gradual reduction in train

speed over a distance of 1 m (produced by form drag and frictional resistance of the air and wire) are likely to influence the measured value of U by less than about 0.5%. Thus, the overall error in the velocity measurement is estimated to be no more than about 1% (or 3 k.p.h. at $U \sim 300$ k.p.h.).

5. Conclusion

The structure of the compression wave generated by a high-speed train entering a tunnel depends principally on portal geometry, the blockage $\mathscr{A}_0/\mathscr{A}$ and the train speed U. The wave amplitude is given approximately by

$$\frac{\rho_0 U^2}{1-M^2}\frac{\mathscr{A}_0}{\mathscr{A}}\left(1+\frac{\mathscr{A}_0}{\mathscr{A}}\right), \quad M=\frac{U}{c_0},$$

and the initial thickness of the compression wave decreases with increasing train Mach number like $1/M$. In a long tunnel nonlinear steepening of the wavefront can ultimately produce rapidly varying pressure transients whose magnitude can exceed 2–3% of the atmospheric pressure. The pulsatile 'micro-pressure wave' radiated from the far end of the tunnel when the compression wave arrives is then comparable in strength to the 'sonic boom' produced by a supersonic aircraft; it causes windows to rattle and is generally an environmental nuisance. The monopole source representing the displacement of air by the advancing train is responsible for the principal characteristics of the compression wave, but we have shown that it is also necessary to take account of second-order, dipole sources in order to make theoretical predictions fully compatible with experiment. The most important dipole source is produced by the pressure drag on the nose of the train. A second contribution of comparable magnitude is generated by 'vortex sound' dipoles in the back-flow of air displaced by the entering train out of the portal. However, this is usually important only after the compression wave is formed, and its effect may in practice be masked by similar contributions from regions of separated flow on the train and tunnel walls that become progressively more significant after entry of the nose into the tunnel.

The harmful effects of nonlinear steepening can be mitigated by increasing the initial thickness of the compression wave. A portal that is 'optimally flared' in accordance with equations (3.7) and (3.8) over a distance ℓ has been predicted theoretically to cause the pressure to increase linearly across the wavefront over a distance $\sim \ell/M$. This conclusion is borne out by our experiments using an optimally profiled portal and an axisymmetric model 'train' travelling at $U \sim 300$ k.p.h. ($M \approx 0.25$) at the relatively large blockage $\mathscr{A}_0/\mathscr{A} = 0.2$. These experiments confirm that linear growth of the compression wave occurs during the time in which the front of the train crosses the flared section of the tunnel, and that for a given length ℓ of the flared section, the overall value of the pressure gradient $\mathrm{d}p/\mathrm{d}t$ is then a minimum. Such a portal therefore provides a potentially effective means of suppressing the micro-pressure wave radiation from the far end of the tunnel.

REFERENCES

Auvity, B. & Bellenoue, M. 1998 Vortex structure generated by a train tunnel entry near the portal. Paper presented at the *8th Intl Symp. on Flow Visualization, Sorrento, Italy, 1–4 September* (ed. G. M. Carlomagno & I. Grant). Edinburgh University.

Ffowcs Williams, J. E. & Hawkings, D. L. 1969 Sound generation by turbulence and surfaces in arbitrary motion. *Phil. Trans. R. Soc. Lond.* A **264**, 321–342.

Fox, J. A. & Vardy, A. E. 1973 The generation and alleviation of air pressure transients caused by the high speed passage of vehicles through tunnels. *BHRA Symp. on the Aerodynamics and Ventilation of Vehicle Tunnels, University of Kent, UK, 10–12 April 1973* (ed. H. S. Stephens, A. L. King & C. A. Richardson), Paper G3, pp. 49–64.

Hara, T. 1961 Aerodynamic force acting on a high speed train at tunnel entrance. *Bull. Japan Soc. Mech. Engrs* **4**(15), 547–553. (Also *Q. Rep. Railway Tech. Res. Inst.* **2**(2), 5–11, 1961.)

Hara, T., Kawaguti, M., Fukuchi, G. & Yamamoto, A. 1968 Aerodynamics of high-speed train. *Mon. Bull. Intl Railway Congr. Assoc.* **XLV**(2), 121–146.

Howe, M. S. 1975 Contributions to the theory of aerodynamic sound, with application to excess jet noise and the theory of the flute. *J. Fluid Mech.* **71**, 625–673.

Howe, M. S. 1998*a* *Acoustics of Fluid-Structure Interactions.* Cambridge University Press.

Howe, M. S. 1998*b* The compression wave produced by a high-speed train entering a tunnel. *Proc. R. Soc. Lond.* A **454**, 1523–1534.

Howe, M. S. 1998*c* Mach number dependence of the compression wave generated by a high-speed train entering a tunnel. *J. Sound Vib.* **212**, 23–36.

Howe, M. S. 1999*a* Review of the theory of the compression wave generated when a high-speed train enters a tunnel. *Proc. Inst. Mech. Engng* F: *J. Rail and Rapid Transit* **213**, 89–104.

Howe, M. S. 1999*b* On the compression wave generated when a high-speed train enters a tunnel with a flared portal. *J. Fluids Struct.* **13**, 481–498.

Iida, M., Matsumura, T., Nakatani, K., Fukuda, T. & Maeda, T. 1996 Optimum nose shape for reducing tunnel sonic boom. *Inst. Mech. Engrs Paper* C514/015/96.

Lamb, H. 1932 *Hydrodynamics*, 6th Edn. Cambridge University Press (Reprinted 1993).

Maeda, T., Matsumura, T., Iida, M., Nakatani, K. & Uchida, K. 1993 Effect of shape of train nose on compression wave generated by train entering tunnel. *Proc. Intl Conf. on Speedup Technology for Railway and Maglev Vehicles, Yokohama, Japan, 22–26 November, 1993, Tokyo University* (ed. M. Iguchi), pp. 315–319. Japan Society of Mechanical Engineers.

Morse, P. M. & Feshbach, H. 1953 *Methods of Theoretical Physics*, Vols 1 and 2. McGraw-Hill.

Ogawa, T. & Fujii, K. 1994 Numerical simulation of compressible flows induced by a train moving into a tunnel. *Comput. Fluid Dyn. J.* **3**, 63–82.

Ogawa, T. & Fujii, K. 1997 Numerical investigation of three dimensional compressible flows induced by a train moving into a tunnel. *J. Computers Fluids* **26**, 565–585.

Ozawa, S. 1979 Studies of micro-pressure wave radiated from a tunnel exit. *Railway Tech. Res. Inst., Japanese National Railways, Rep.* 1121 (in Japanese).

Ozawa, S. & Maeda, T. 1988 Model experiment on reduction of micro-pressure wave radiated from tunnel exit. In *Proc. Intl Symp. on Scale Modeling, Tokyo, 18–22 July, Seikei University* (ed. R. I. Emori). Japan Society of Mechanical Engineers.

Ozawa, S., Maeda, T., Matsumura, T., Uchida, K., Kajiyama, H. & Tanemoto, K. 1991 Countermeasures to reduce micro-pressure waves radiating from exits of Shinkansen tunnels. In *Aerodynamics and Ventilation of Vehicle Tunnels,* pp. 253–266. Elsevier.

Ozawa, S., Tsukamoto, K. & Maeda, T. 1976 Model experiments on devices to reduce pressure wave radiated from a tunnel. *Railway Tech. Res. Inst., Japanese National Railways, Rep.* 990 (in Japanese).

Rayleigh, Lord 1926 *The Theory of Sound*, Vol. 2. Macmillan.

Sugimoto, N. 1994 Sound field in a tunnel generated by a traveling high speed train. *Theor. Comput. Acoust.* **1**, 45–56.

Sugimoto, N. & Ogawa, T. 1998 Acoustic analysis of the pressure field in a tunnel, generated by entry of a train. *Proc. R. Soc. Lond.* A **454**, 2083–2112.

Woods, W. A. & Pope, C. W. 1976 Secondary aerodynamic effects in rail tunnels during vehicle entry. *Second BHRA Symp. on the Aerodynamics and Ventilation of Vehicle Tunnels, Cambridge* (ed. H. S. Stephens, R. Rosemary Dowden, A. L. King & M. P. Patel), *UK, 23–25 March 1976*, Paper C5, pp. 71–86.